# Weierstraß-Institut
## für Angewandte Analysis und Stochastik
### Leibniz-Institut im Forschungsverbund Berlin e. V.

Preprint ISSN 2198-5855


# Dispersive time-delay dynamical systems


Alexander Pimenov [1], Svetlana Slepneva [2,3], Guillaume Huyet [2,3,4], Andrei G. Vladimirov [1,5]



submitted: October 31, 2016



[1] Weierstrass Institute
Mohrenstr. 39
10117 Berlin
Germany
E-Mail: alexander.pimenov@wias-berlin.de
andrei.vladimirov@wias-berlin.de

[2] Tyndall National Institute
University College Cork
Lee Maltings, Dyke Parade
Cork
Ireland

[3] Centre for Advanced Photonics and Process Analysis and
Department of Applied Physics and Instrumentation
Cork Institute of Technology
Cork
Ireland

[4] National Research University of
Information Technologies, Mechanics and Optics
199034 St Petersburg
Russia

[5] Lobachevsky State University
Gagarina av. 23
603950 Nizhny Novgorod
Russia



No. 2324
Berlin 2016



2010 *Physics and Astronomy Classification Scheme.* 42.60.Mi, 42.65.Sf, 42.55.Ah, 42.55.Px.

*Key words and phrases.* Time-delay systems, chromatic dispersion, laser dynamics, FDML, modulational instability.

The authors thank Stephen P. Hegarty, Sergio Rica, Julien Javaloyes, Svetlana Gurevich, Shalva Amiranashvili, and Dmitry Turaev for fruitful discussions and useful advices. AP and AGV acknowledge the support of SFB 787 of the DFG. AGV acknowledges the support of the Grant No. 14-41-00044 of the Russian Science Foundation. GH acknowledges Science Foundation Ireland under Contract No. 11/PI/1152. SS gratefully acknowledges the support of the EU FP7 Marie Curie Action FP7-PEOPLE-2010-ITN through the PROPHET project, Grant No. 264687.

Edited by
Weierstraß-Institut für Angewandte Analysis und Stochastik (WIAS)
Leibniz-Institut im Forschungsverbund Berlin e. V.
Mohrenstraße 39
10117 Berlin
Germany

Fax: +49 30 20372-303
E-Mail: preprint@wias-berlin.de
World Wide Web: http://www.wias-berlin.de/

**Abstract**

We present a theoretical approach to model the dynamics of a dispersive nonlinear system using a set of delay differential equations with distributed delay term. We illustrate the use of this approach by considering a frequency swept laser comprising a semiconductor optical amplifier (SOA), a tunable bandpass filter and a long dispersive fiber delay line. We demonstrate that this system exhibits a rich spectrum of dynamical behaviors which are in agreement with the experimental observations. In particular, the multimode modulational instability observed experimentally in the laser in the anomalous dispersion regime and leading to a turbulent laser output was found analytically in the limit of large delay time.

# 1 Introduction

Time-Delay Dynamical Systems (TDDS) have been successfully used to describe a variety of problems ranging from population and neural dynamics in biological sciences [4,5,22] to short pulse formation and appearance of instabilities in laser physics [13, 16, 18, 26]. They also appear in control [19], modelling of climate [10], modern computational methods [3,17], and the dynamics of coupled oscillators [11,12]. In each of these problems, delay is a direct consequence of wave propagation without dispersion. However, waves of different physical origin such as electromagnetic, acoustic, or water waves are subject to dispersion when propagating in a medium with the phase velocity depending on the frequency of the wave. In nonlinear medium the interplay between dispersion and nonlinearity can give rise to a modulational instability [28] and soliton formation [29]. A commonly adopted approach to describe these phenomena is based on the application of NLS and CGLE-type equations where the second and higher order chromatic dispersions are described by time derivatives of different orders. This letter aims to provide a framework to study the effect of chromatic dispersion on the dynamics of TDDS.

# 2 Chromatic dispersion in TDDS

In the case of TDDS model equations depend not only on the current state vector $\mathbf{U}(t)$, but also on the past states $U_k(t-T_k)$, where $T_k$ are the delay times, $k=1,...,n$. Without the loss of generality we can assume that we have only a single delayed variable $U_1(t-T)$ and a single delay time $T_1=T$ in the model equations. To introduce chromatic dispersion we first consider a complex variable $u(t,z)=u(t-z/c,0)$ satisfying linear homogeneous unidirectional wave equation $(1/c)u_t+u_z=0$ on the interval $0\le z\le L$ and postulate that the current state variable $U_1(t)$ and its delayed value are given, respectively, by the values of $u(t,z)$ at the beginning and at the end of the dispersionless delay line of length $L=cT$, $U_1(t)\equiv u(t,0)$ and $U_1(t-T)\equiv u(t,L)=u(t-T,0)$. Next, when the dispersion is present we replace the homogeneous wave equation with non-homogeneous one:

$$\frac{1}{c}\frac{\partial u}{\partial t}+\frac{\partial u}{\partial z}=p(t,z), \tag{1}$$

where $p$ is the linear "polarization" describing the dispersive properties of the delay line medium. In the frequency domain $\hat{p}$ is proportional to $\hat{u}(\omega,z)$ via the susceptibility $\chi(\omega,z)$ as

$$\hat{p}(\omega,z)=\chi(\omega,z)\hat{u}(\omega,z). \tag{2}$$

Equations (1) and (2) are integrated in the co-moving reference frame ($t' = t - z/c$ and $z' = z$) in order to obtain $\hat{u}(\omega, L)$

$$\hat{u}(\omega, L) = \hat{u}(\omega, 0) e^{\int_0^L \chi(\omega, z) dz}, \tag{3}$$

and $u(t, L)$ is obtained by performing the inverse-Fourier transform of (3).

In this paper, we assume that $\chi(\omega, z) = \chi(\omega)$ is homogeneous in $z$, hence without loss of generality $\chi(\omega)$ can be decomposed in a sum of Lorentzians

$$\chi(\omega) = -\int \frac{n(\omega_0)}{\Gamma(\omega_0) + i(\omega + \omega_0)} d\omega_0, \tag{4}$$

where $n(\omega_0)$ is the density of states.

For a single Lorentzian,

$$\chi(\omega) = \frac{-\sigma}{\Gamma + i(\omega + \Omega)}, \tag{5}$$

with central frequency $\Omega$ and full-width at half-maximum $\Gamma$, corresponding to $n(\omega_0) = \sigma\delta(\omega_0 - \Omega)$, one can write

$$u(t, L) = u(t - T, 0) + P(t - T) = U_1(t - T) + P(t - T), \tag{6}$$

where

$$P(t) = \sigma L \int_{-\infty}^{t} e^{-(\Gamma + i\Omega)(t-s)} \frac{J_1\left[\sqrt{4\sigma L(t-s)}\right]}{\sqrt{\sigma L(t-s)}} u(s, 0) ds. \tag{7}$$

The relation (6) gives an expression for the output field from the dispersive delay line. Therefore, in order to account for the effect of dispersion in the model equations we need to replace in these equations the output field $U_1(t - T)$ from a dispersionless delay line with that calculated in the presence of chromatic dispersion: $U_1(t - T) + P(t - T)$. The resulting set of equations with distributed delay describes the behaviour of the TDDS in the presence of dispersion and the usual tools of non-linear dynamics theory can be applied to study the stability and bifurcations of various solutions.

## 3 Experimental study of a FDML laser

To illustrate the application of our method to a specific physical problem, we shall now consider the example of a ring laser with a long dispersive fiber line and compare the experimental results with those obtained theoretically. Such a laser operating in Fourier Domain Mode-Locking (FDML) regime [8] generates frequency swept light commonly used in Optical Coherence Tomography and can be described by a set of two DDE's [20]. In addition, it has recently been shown that the coherence properties of this laser depend strongly on the dispersion of the fiber delay line [1].

The schematic of the experimental setup is shown in Fig. 1(a) (it is the same as in [20]). The gain medium was provided by an SOA (Thorlabs, BOA1132) with an amplified spontaneous emission peak wavelength of 1303.8nm. A tunable element was a Fabry-Pérot tunable narrow band (50 pm) optical bandpass filter (MicronOptics) with about 20 THz free spectral range. The filter transmission was controlled by an AC source. The isolator incorporated into the cavity ensured unidirectional propagation of light and excluded any parasitic back reflections. The overall cavity length, mostly formed by the fiber pigtails of the cavity components, was estimated 17m. The amount of dispersion was controlled by including additional SMF fiber delays of various lengths thus allowing for the cavities ranging from 17m to 20km. For the 20km cavity length the wavelength of the minimum group velocity of the system was measured 1317nm. The laser dynamics was analysed by a DC-coupled broadband 12 GHz photoreceiver (Newport, 1554-B) and a real time oscilloscope of 12 GHz bandwidth.

When the filter transmission was set at a fixed wavelength (static regime) within the range of the normal dispersion (i.e. wavelengths below 1317nm), the laser exhibited bistability demonstrating a random switching between the constant wave (CW) and chaotic solutions as shown in Fig. 1(c). A minor shift of the filter transmission towards longer wavelengths stabilised the CW solution while a shift towards shorter wavelengths destabilised the CW solution giving way to a turbulent output. The observed hysteresis lead to the asymmetry of the laser intensity for the case when the filter transmission was periodically modulated at a slow frequency (quasi-static regime) to scan a range of wavelengths in the normal dispersion region. This is illustrated in Fig. 2(a). The top black curve schematically shows the direction of the filter sweep near its turning point (corresponds to 0 value on the time axis) where the filter was changing its transmission wavelength from the decreasing (negative time values) to increasing (positive time values). The time trace (a) shows the change in the laser intensity depending on the sweep direction: for the decreasing wavelengths the laser displayed chaotic oscillations while the increase of the wavelengths lead to a series of the power dropouts. The stability analysis for this case is presented in [20].

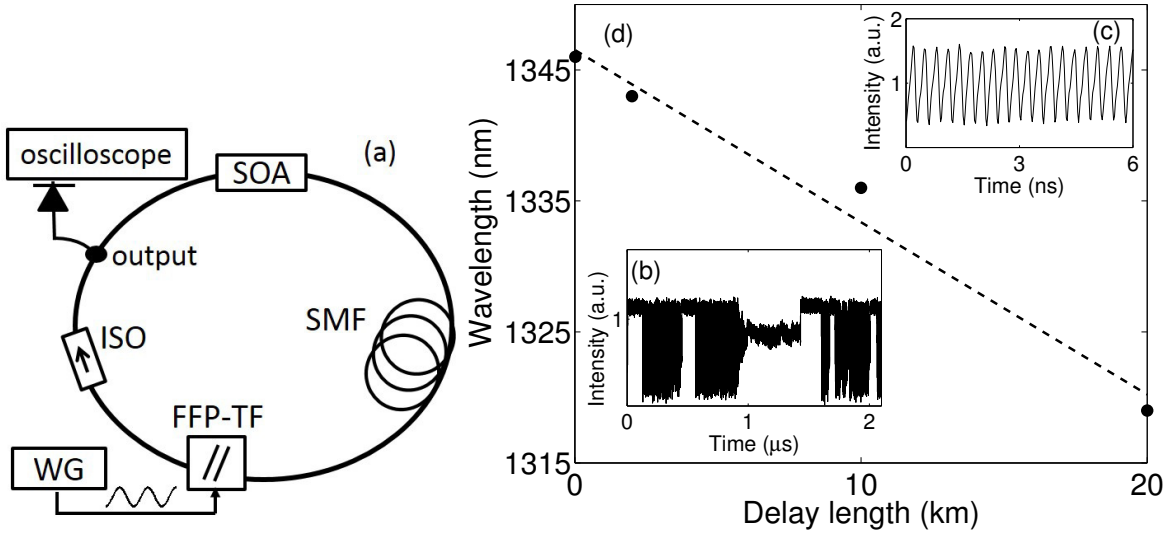


Figure 1: (a) Experimental set-up of the ring laser. SOA: Semiconductor Optical Amplifier; ISO: Isolator; SMF: Single Mode Fiber (0m, 300m, 2km, 10km, 20km); FFP-TF: Fiber Fabry-Pérot Tunable Filter; WG: waveform generator. (More details on the components can be found in [20]). (b) Bistability between the chaos and CW observed at a static wavelength for the case of the normal dispersion. (c) Chaotic dynamics observed at a static wavelength for the case of the anomalous dispersion. (b) Threshold division for the modulational instability for various fiber lengths. The bistability regime is observed to the left of the threshold line and chaos to its right.

When the filter transmission was set at a fixed wavelength in the range of the anomalous dispersion, the laser output remained always chaotic as shown in Fig. 1(d), and was not influenced by any slight variations of the filter transmission. When the filter was quasi-statically tuned in the region of the anomalous dispersion, the laser output showed a strong dependence on the filter speed: at a slow modulation frequency the laser exhibited chaotic output regardless of the sweep direction (Fig. 2(b)) while as the filter modulation frequency increased, an asymmetry appeared (Fig. 2(c)), however, the CW output had never been stabilized.

These results indicated the influence of the fiber dispersion on the stability of the laser. To investigate this point further, the wavelength at which the transition from the bistable to chaotic dynamics occurred was measured as a function of the cavity length (Fig. 1(c)). In particular, for the cavity length of 20km, the transition occurred at 1346nm while the minimum system group delay was measured 1317nm, thus demonstrating that the laser can become chaotic even without dispersion. The fact that the CW solution was no longer observed at long

wavelengths indicated that the dispersion led to an additional instability.

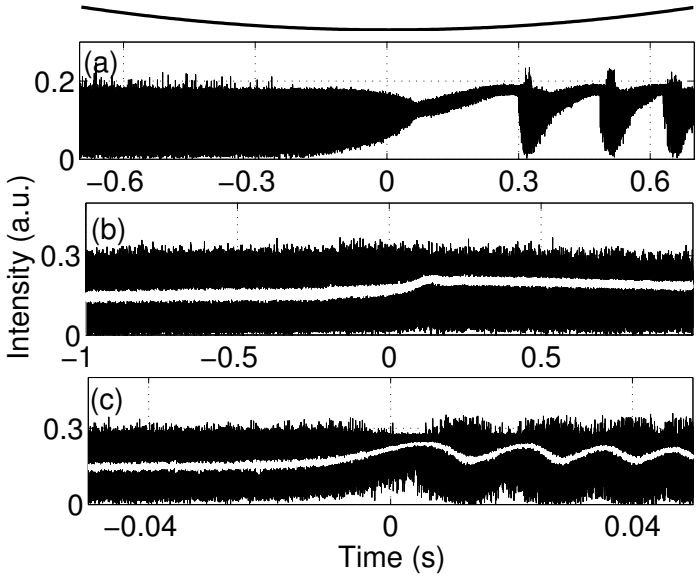


Figure 2: Experimentally measured dynamics of the laser operating in a quasi-static regime at the turning point of the filter transmission (the top curve) for the case of (a) the normal dispersion region (tuning around 1303nm, 100mHz modulation frequency); (b) the anomalous dispersion region (tuning around 1328nm, 200mHz modulation frequency); (c) the anomalous dispersion region (1600mHz modulation frequency). Black: the intensity measured with 12GHz bandwidth, white: the numerically filtered intensity.

# 4 Theoretical analysis of a FDML laser

## 4.1 Time-delay model

To model this system theoretically, let us consider a laser consisting of an SOA as an amplifying medium, a tunable spectral filter, and a dispersive fiber delay line in a ring cavity. We assume that the chromatic dispersion of the delay line material is caused by a Lorentzian absorption line with the central frequency detuned with respect to the reference frequency associated with the central wavelength of the amplification line of the SOA. Using this approach we can describe both the case of normal dispersion (blue-shifted absorption line, positive detuning $\Omega > 0$ in (5)) and anomalous dispersion case (red-shifted absorption line, negative detuning $\Omega < 0$ in (5)). We use the lumped element approach similar to that applied in [26], and apply the formalism discussed above to describe the propagation of light in a dispersive medium with detuned Lorentzian absorption line using the equation (6), where $u(t,z)$ represents the slowly varying electric field envelope in the delay line. Then assuming that the total length of the SOA and tunable filter can be neglected as compared to the delay line length $L = cT$, we derive the following set of DDEs for the complex envelope of the electric field at the entrance of the SOA, $A(t)$, and the saturable gain of the SOA, $G(t)$ [25]:

$$\frac{dA}{dt} + (\gamma - iw)A = \gamma\sqrt{\kappa}e^{(1-i\alpha)G/2}\left[A_T + P_T\right], \tag{8}$$

$$\frac{dG}{dt} = \gamma_g\left[g_0 - G - (e^G - 1)\left|A_T + P_T\right|^2\right], \tag{9}$$

where $A_T = A(t-T), P_T = P(t-T)$, $T$ is the cold cavity round trip time, $\gamma$ is the tunable filter width, $w$ is the relative position of the central frequency of this filter. The parameters $\kappa$, $\alpha$, and $g_0$ describe, respectively, attenuation factor related to nonresonant loss per cavity round trip, linewidth enhancement factor, and the pump parameter. Finally,

$$P(t) = -d \int_{-\infty}^{t} e^{-(\Gamma+i\Omega)(t-s)} \frac{J_1\left[\sqrt{4d(t-s)}\right]}{\sqrt{d(t-s)}} A(s) ds. \tag{10}$$

where $d = \sigma L$. In the case of zero dispersion $P = 0$ the DDE system (8) and (9) contains a single discrete delay and coincides with model equations studied in [20, 21].

## 4.2 Stability analysis of CW solutions

To investigate theoretically the appearance of modulational instability in the system (8)-(10) let us consider a CW solution in the form $A(t) = A_0 e^{i\nu t}$ and $G(t) = G_0$, which together with (7) imply $P(t) = \left(e^{-d/[\Gamma+i(\Omega+\nu)]} - 1\right) A_0 e^{i\nu t}$. Substituting these relations into (9) and (8) we obtain the following expression for the CW intensity and stationary value of the carrier density

$$|A_0|^2 = \frac{g_0 - G_0}{e^{G_0} - 1} e^{\frac{2d\Gamma}{\Gamma^2+(\Omega+\nu)^2}}, \tag{11}$$

$$G_0 = \ln\left[\frac{\gamma^2 + (w-\nu)^2}{\gamma^2 \kappa} e^{\frac{2d\Gamma}{\Gamma^2+(\Omega+\nu)^2}}\right], \tag{12}$$

where the frequencies $\nu$ of CW solutions satisfy a transcendental equation.

Next, following the approach described in [27] we perform linear stability analysis of CW solutions (11)-(12) in the limit $T \to \infty$. We linearize the system near the steady state $A = \left(A_0 + \delta A e^{\lambda t}\right) e^{i\nu t}$, $G = G_0 + \delta G e^{\lambda t}$, and $P_1 = \left(P_0 + \delta P e^{\lambda t}\right) e^{i\nu t}$, with the relation $\delta P = \delta A \left(e^{-d/[\Gamma+\lambda+i(\Omega+\nu)]} - 1\right)$ following from (7). Then we can obtain the following characteristic equation for the eigenvalues $\lambda$ describing the stability of CW solutions:

$$a(\lambda) Y(\lambda T)^2 + b(\lambda) Y(\lambda T) + c(\lambda) = 0, \tag{13}$$

where $Y(\lambda T) = e^{-\lambda T}$, and $a(\lambda), b(\lambda), c(\lambda)$ are coefficients independent of the delay time $T$ (see Appendix A).

Finally, in the limit of large delay time $T \to \infty$ we can represent the eigenvalues belonging to the pseudo-continuous spectrum in the form $\lambda = i\mu + \frac{\Lambda}{T} + \mathcal{O}(1/T^2)$ with real $\mu$ [27]. Then, keeping only the single leading term $i\mu$ in $a(\lambda)$,$b(\lambda)$, $c(\lambda)$ and two leading terms $i\mu + \frac{\Lambda}{T}$ in $Y(\lambda T)$, we obtain two branches of pseudo-continuous spectrum $\Lambda_{\pm}(\mu)$. Real parts of these eigenvalue branches are shown in Fig. 3 (a) indicating the presence of modulational instability in the anomalous dispersion regime. As it can be seen from Fig. 3(a), appearance of the modulational instability is associated with the change of the sign of the curvature of one of the two eigenvalue branches at the origin $\mu = 0$, which allows us to derive analytically the condition for modulational instability of the CW solution [25, 27]

$$-\left(\frac{\gamma - \alpha(w-\nu)}{\gamma^2 + (w-\nu)^2}\right)^2 - \alpha D_2 + F(w, \nu, d, \Omega) > 0, \tag{14}$$

where second-order dispersion coefficient is represented by

$$D_2 = \mathrm{Im}\, \frac{\mathrm{d}^2}{\mathrm{d}\nu^2} \left(\frac{-d}{\Gamma + i(\Omega+\nu)}\right).$$

Here the last term in the left hand side is almost independent of the chromatic dispersion above the lasing threshold for $|\Omega| \gg 1$: $F(w, \nu, d, \Omega) \approx F(w, \nu, 0, \Omega)$. In the absence of dispersion this term is responsible for the appearance of modulational instability at negative detunings $w < \nu$, which is symmetric with respect to the zero detuning point $\nu = w$, $F(w, w, 0, \Omega) = 0$ and $F(w, w + \delta\nu, 0, \Omega) = F(w, w - \delta\nu, 0, \Omega)$ [20] (see Appendix A).

In the absence of dispersion ($d = D_2 = 0$) a CW solution is always stable with respect to modulational instability when the central frequency of the spectral filter is tuned exactly to the frequency of this solution, $w = \nu$ ($-\frac{1}{\gamma^2} < 0$) [20]. In the case of dispersive delay line $d > 0$, the necessary condition for the modulational instability at $w = \nu$ is

$$\alpha D_2 < -\frac{1}{\gamma^2}. \tag{15}$$

This condition resembles the modulational instability criterion for the complex Ginzburg-Landau equation [24]. The sign of the second-order dispersion coefficient $D_2$ is determined by the sign of $\Omega$ for large enough $|\Omega| > \Gamma\sqrt{3}$. In particular, modulational instability (15) occurs only for the case of anomalous dispersion $\Omega < 0$.

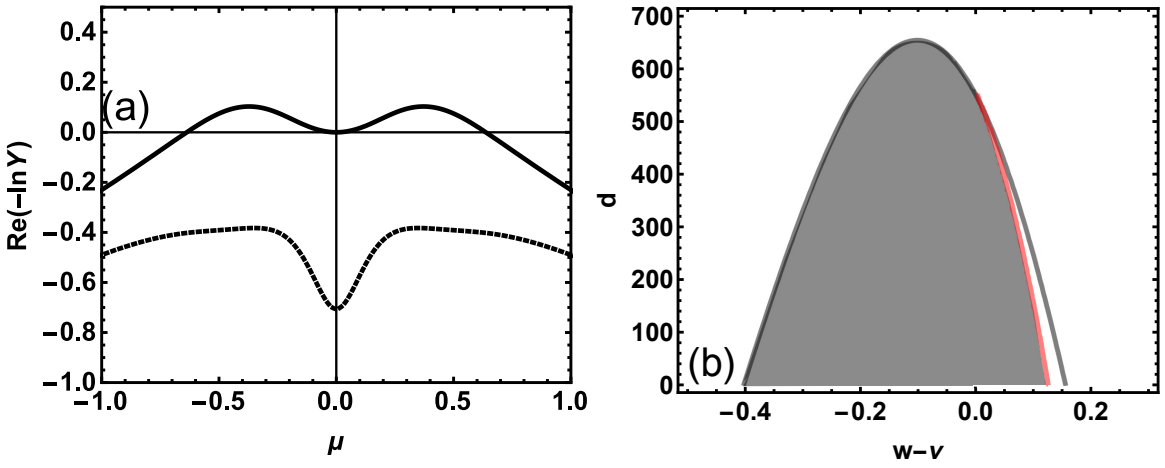


Figure 3: (a) Real parts of two branches of the pseudo-continuous spectrum $\mathrm{Re}\Lambda_{\pm}(\mu)$ in the case of strong anomalous dispersion, $\Omega = -13$, $d = 1000.0$, $\nu = 0$. (b) Modulational instability boundary (black) and Turing-like instability boundary (light/red color) in anomalous dispersion regime on the plane of two parameters, dispersion strength $d$ and the relative frequency of the CW regime $w - \nu$. The gray region denotes stable CW solutions. Other parameter values: $\gamma = 1$, $g_0 = 3.0$, $\alpha = 2$, $\kappa = 0.2$, $\gamma_g = 0.1$, $w = 0$, and $\Gamma = 0.001$.

Stability analysis of the CW solution (11) for various values of $w - \nu$ in the static regime $w = const$ allows us to understand the asymmetry of the dynamical output of the laser with respect to the sweeping direction in the quasi-static and FDML regimes [20]. Indeed, in the case of moderate normal or weak anomalous dispersion (see Fig. 3(b)), similarly to the case without dispersion, for $w > \nu$ we observe a Turing-type instability of the CW solution, which leads to a jump from one longitudinal mode to another for positive sweep direction, whereas for $w < \nu$ and sufficiently high $\alpha$-factor CW regime looses stability via a weak modulational instability, which results in the chaotic output of the laser for negative sweep direction [20]. It can be seen from Fig. 3b that, when the strength of the anomalous dispersion $d$ is increased above a certain threshold, the Turing-type instability at $w > \nu$ is replaced by modulational instability, so that for both signs of the detuning $w - \nu$ the CW solution is destabilized via a modulational instability. With further increase of the dispersion strength two modulational instability boundaries in Fig. 3b merge with one another and the CW regime becomes always unstable for any values of $w - \nu$. Noteworthy, examination of first two terms in (14) implies that for $w > \nu$ the modulational instability threshold value of the dispersion strength is lower, and for some $0 < \nu - w < \alpha\gamma$ it is higher than for $\nu = w$. This explains the asymmetry of the black curve in Fig. 3(b) with respect to $w - \nu = 0$.

### 4.3 Numerical simulations

To investigate the effect of anomalous dispersion on the dynamics of FDML laser in the quasi-static regime numerically, we assumed that the central frequency of the filter is swept periodically in time, $w = w(t) = \Delta \sin \rho t$ [20], where $\rho \ll 1$. In our simulations the narrow filter was swept over the window of several filter bandwidths. In order to keep second-order dispersion constant inside the sweeping window we chose the central frequency of the Lorentzian $\Omega = \pm 13\gamma + w$ moving together with the central frequency of the filter. The effect of normal and anomalous dispersion on symmetry properties of the FDML laser output with respect to the sweep direction is illustrated by Fig. 4. In particular, it can be seen from Fig. 4(c) that for $d = 600\gamma$, when the small interval of detunings $w - \nu$, where the CW regime is stable, is limited by two modulational instability points (see Fig. 3(b)), a chaotic output is observed for both sweep directions at low sweep speed $\rho = 10^{-7}$. On the contrary, for higher sweep speed $\rho = 5 \times 10^{-6}$ one can see a weak attraction towards a CW regime and corresponding jumps in the numerically filtered field intensity $|A|^2(t)$, see Fig. 4(b) that match closely the jumps shown in Fig. 4(a) for the case of normal dispersion. Thus, our numerical results are in good qualitative agreement with the experimental results presented in Fig. 2.

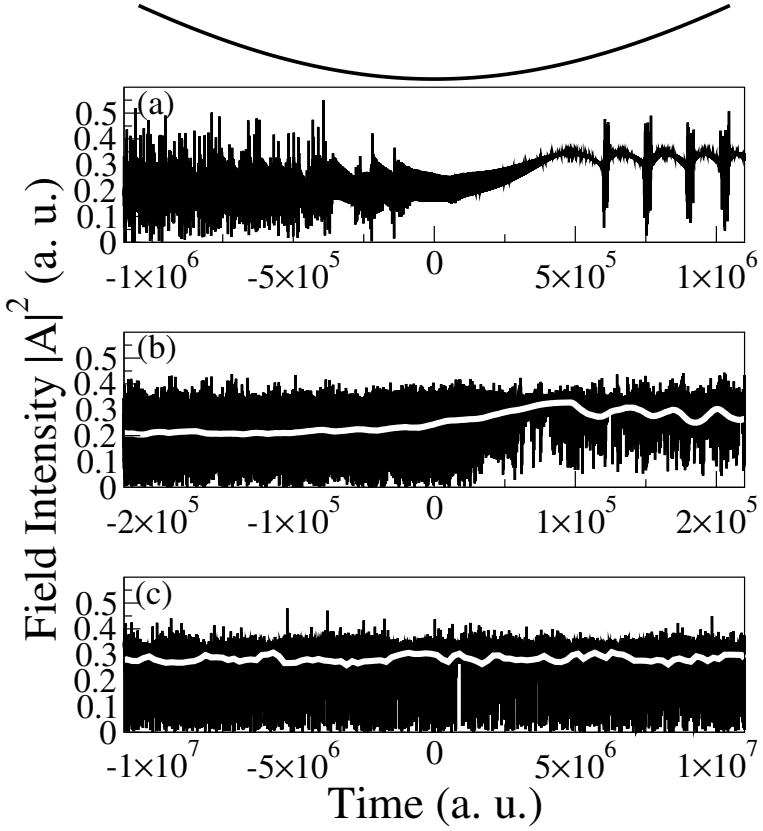


Figure 4: Numerical solution of the system (8)-(10) for $\Delta(t) = \Delta_0 \sin \rho t$ at the turning point of the filter transmission $\sin \rho t = -1$ (top) in case of (a) normal dispersion $\Omega = 13$ (modulation frequency $\rho = 10^{-6}$); (b) anomalous dispersion $\Omega = -13$ (modulation frequency $\rho = 5 \times 10^{-6}$); (c) anomalous dispersion $\Omega = -13$ and modulation frequency $\rho = 10^{-7}$. The black traces are the recorded time traces and the white traces are numerically filtered signals. Here, $d = 600$, $\Delta = 5$, and other parameters are as in Fig. 3. Numerical discretization of the system (8)-(9) was performed using Heun's method, where the integral (10) was calculated using Levin's method for highly oscillatory integrals [14] (see Appendix B).

# 5 Conclusion

To conclude, we have provided a theoretical framework to describe the effect of dispersion in a non-linear system modelled by a set of DDEs. This approach was applied to successfully describe the emergence of modulation instability observed experimentally in a ring cavity laser containing a long fibre delay line. In particular, we have shown that in the anomalous dispersion regime the dispersion of the fiber delay line can destabilize the CW laser operation leading to a turbulent behavior. We believe that this framework could be used to investigate the impact of dispersion on the dynamics of a broad class of systems commonly described by DDE's. For example, this approach could be used to understand the effect of linear chromatic dispersion on the characteristics of mode-locked regime in monolithic multi-section lasers and other non-linear photonic devices [2,3,6,7,9,15,16,18,23]. Our framework can be also applied to much more general systems like Stuart-Landau equation with delayed feedback [9] (see Appendix C).

# 6 Appendix A. Modulational instability in the delayed model of FDML laser

We consider the characteristic equation (13) for the eigenvalues $\lambda$ describing the stability of CW solution $A(t) = A_0 e^{i\nu t}$, where

$$a(\lambda) = -\gamma^2\kappa e^{G_0 - \frac{2a\Gamma L(\Gamma+\lambda)}{(\Gamma+\lambda)^2+(\nu+\Omega)^2}} \left[\lambda + \gamma_g\left(1 + |A_0|^2 e^{-\frac{2a\Gamma^2 L}{\Gamma^2+(\nu+\Omega)^2}}\right)\right],$$

$$c(\lambda) = -\left[(\gamma+\lambda)^2 + (w-\nu)^2\right]\left[\lambda + \gamma_g\left(1 + |A_0|^2 e^{G_0 - \frac{2a\Gamma^2 L}{\Gamma^2+(\nu+\Omega)^2}}\right)\right],$$

$$b(\lambda) = e^{-\frac{a\Gamma L(\Gamma+\lambda)}{(\Gamma+\lambda)^2+(\Omega+\nu)^2}} \left\{p(\lambda)\cos\left[\Psi - \Theta(\lambda)\right] + q(\lambda)\sin\left[\Psi - \Theta(\lambda)\right]\right\},$$

$$p(\lambda) = \gamma e^{G_0/2}\sqrt{\kappa}\left\{2(\gamma_g+\lambda)(\gamma+\lambda) + \gamma_g|A_0|^2 e^{-\frac{2a\Gamma^2 L}{\Gamma^2+(\nu+\Omega)^2}}\left[\left(e^{G_0}+1\right)(\lambda+\gamma) + \alpha\left(e^{G_0}-1\right)(\nu-w)\right]\right\},$$

$$q(\lambda) = \gamma e^{G_0/2}\sqrt{\kappa}\left\{2(\gamma_g+\lambda)(w-\nu) + \gamma_g|A_0|^2 e^{-\frac{2a\Gamma^2 L}{\Gamma^2+(\nu+\Omega)^2}}\left[\left(e^{G_0}+1\right)(w-\nu) + \alpha\left(e^{G_0}-1\right)(\gamma+\lambda)\right]\right\},$$

and

$$\Psi = \frac{\alpha G_0}{2} + \nu T, \quad \Theta(\lambda) = \frac{a\Gamma L(\nu+\Omega)}{(\Gamma+\lambda)^2 + (\nu+\Omega)^2}.$$

In the limit of large delay two branches of pseudo-continuous spectrum $\Lambda_\pm(\mu)$ are given by

$$\Lambda_\pm(\mu) + i\mu T = -\ln\left[\frac{-b(i\mu) \pm \sqrt{b(i\mu)^2 - 4a(i\mu)c(i\mu)}}{2a(i\mu)}\right]. \tag{16}$$

Therefore, we assume $y(\mu) = -\operatorname{Re}\ln\hat{Y}(\mu)$, $\hat{Y}(\mu) = Y(i\mu)$, hence the modulational instability threshold can be found using the condition $y''(0) = 0$. Since

$$y''(0) = \operatorname{Re}\left[\frac{\hat{Y}'(0)^2}{\hat{Y}(0)^2} - \frac{\hat{Y}''(0)}{Y(0)}\right],$$

we can find $\hat{Y}(0)$, $\hat{Y}'(0)$, $\hat{Y}''(0)$ from (13), first and second derivative of (13) at $\mu = 0$. One can see that for the corresponding branch of eigenvalues $\hat{Y}(0) = 1$,

$$\hat{Y}'(0) = i\left[\frac{\gamma - \alpha(w-\nu)}{\gamma^2 + (w-\nu)^2} + \frac{d}{\Gamma^2 + (\Omega+\nu)^2}\left(1 - \frac{2\Gamma\big(\Gamma - \alpha(\Omega+\nu)\big)}{\Gamma^2 + (\Omega+\nu)^2}\right)\right],$$

and, finally, we obtain the condition (14) for modulational instability above the lasing threshold, where $F = -r_s + r_u$,

$$D_2 = \frac{2d(\Omega+\nu)\big(-3\Gamma^2 + (\Omega+\nu)^2\big)}{\big(\Gamma^2 + (\Omega+\nu)^2\big)^3},$$

$$r_s = \frac{2d\Gamma\big(3(\Omega+\nu)^2 - \Gamma^2\big)}{\big(\Gamma^2 + (\Omega+\nu)^2\big)^3} > 0,$$

$$r_u = \big(1+\alpha^2\big)\left[\left(\frac{w-\nu}{\gamma^2 + (w-\nu)^2}\right)^2 + \left(-1 + \frac{2}{r_1} + \frac{2}{r_2}\right)\left(\frac{w-\nu}{\gamma^2 + (w-\nu)^2} - \frac{2d\Gamma(\Omega+\nu)}{(\Gamma^2 + (\Omega+\nu)^2)^2}\right)^2\right].$$

Here, $r_1$ and $r_2$ are the parts of the CW field $A_0 = \sqrt{\frac{r_1\kappa}{r_2}}$, where

$$r_2 = \frac{\gamma^2 + (w-\nu)^2}{\gamma^2} - \kappa \exp\frac{-2d\Gamma}{\Gamma^2 + (\Omega+w)^2},$$

$$r_1 = g_0 + \ln\kappa + \ln\frac{\gamma^2}{\gamma^2 + (w-\nu)^2} - \frac{2d\Gamma}{\Gamma^2 + (\Omega+\nu)^2}.$$

One can see that the term $r_s > 0$ increases MI threshold, however for $\Omega \gg 1$ this term is small ($r_s \ll 1$). The term $r_u$ destabilizes the CW regime at $w = \nu$ for any type of dispersion (normal or anomalous) in a small vicinity of the lasing threshold where $0 < g_0 + \ln\kappa - 2d\Gamma/\big(\Gamma^2 + (\Omega+\nu)^2\big) \ll \min(\Gamma, \frac{1}{\Gamma})$ and $y''(0) > 0$ (for $\Omega \gg 1$ we have to assume $\Gamma \ll 1$ in order to avoid unrealistically large losses at $\nu = w$, hence this vicinity is negligibly small). For larger $g_0$ the term $r_u$ becomes sufficiently small and the CW regime gains stability ($y''(0) < 0$) till another modulational instability threshold is reached ($y''(0) > 0$) and the CW regime is destabilized once again.

# 7 Appendix B. Numerical simulations of FDML model

In our simulations, we are interested in the effect of second-order dispersion on the dynamics of the laser, hence we choose our parameters in order to maximize the magnitude of second-order dispersion parameter $D_2$ and to minimize all other effects of the Lorentzian dispersion line (10). In particular, we assume $\Omega \gg 1$ large enough so that the Lorentzian is outside of the gain profile, and $\Gamma \ll 1$ to minimize the losses due to Lorentzian absorption line. Finally, we solve the equation (8) in the reference frame of the filter $A := Ae^{i\int \Delta(t)dt}$ by approximating the original system with the system

$$\frac{dA}{dt} + \gamma A = \gamma\sqrt{\kappa}e^{(1-i\alpha)G/2 + i\varphi - i\int_{t-T}^{T}\Delta(s)ds}\left[A_T + P_T\right], \tag{17}$$

(9),(10). The approximation is valid for very slow sweep speed $\Delta'(t) \sim \rho \ll 1$ under assumption of varying $\Omega = \Omega_0 + \Delta(t)$. We note that the last assumption is purely technical and allows us to consider smaller values of $\Omega$ and larger discretization steps. Numerical solution of original system (8)-(9),(10) with fixed large $\Omega$ gives us qualitatively similar results for the same discretization steps, which are subject to higher numerical noise that limits our understanding of the underlying dynamics.

### 7.1 Levin's method for highly oscillatory integrals

It is possible to apply Levin's method [14] for numerical evaluation of highly oscillatory integrals to the integral (10). For that, we consider this integral at a finite interval $[0, mT]$ of $m$ delays, and make a change of variable under the integral $s := \sqrt{s}$ to obtain the integral in the following form

$$P(t) = -\sqrt{d}\int_0^{\sqrt{mT}} A(t-s^2/4)e^{-(\Gamma+i\Omega)s^2/4}J_1\left[\sqrt{d}s\right]ds = \sum_{j=1}^{M}\int_{\sqrt{t_{j-1}}}^{\sqrt{t_j}} f(s)g(s)ds, \qquad f(s) = (0, A(t-s^2/4)),$$

where $t_j$ are points of discretization, $f(s)$ is a slow function, and the highly oscillatory kernel $g(s)$ satisfies a linear system of ODEs with variable coefficients

$$g'(s) = B(s)g(s), \quad B(s) = \begin{pmatrix} -(\Gamma+i\Omega)\frac{s}{2} & -\sqrt{d} \\ \sqrt{d} & -(\Gamma+i\Omega)\frac{s}{2} - \frac{1}{s} \end{pmatrix}.$$

We look for the function $p(s)$ such that $(p^T(s)g(s))' \approx f(s)g(s)$, then the integral can be approximated by

$$\int_{\sqrt{t_{j-1}}}^{\sqrt{t_j}} f(s)g(s)ds \approx p^T(\sqrt{t_{j-1}})g(\sqrt{t_{j-1}}) - p^T(\sqrt{t_j})g(\sqrt{t_j}).$$

From the relation $(p^T(s)g(s))' = p^{T'}g + p^Tg' = (p' + B^Tp)^Tg \approx f(s)g(s)$ it follows that $p \approx q$, where $q$ is the solution of the inhomogeneous linear system

$$q' + B^Tq = f.$$

We solve this system numerically using a collocation method.

## 8 Appendix C. Modulational instability in Stuart-Landau equations with dispersive delayed feedback

We can use the proposed approach to include the effect of chromatic dispersion into the universal Stuart-Landau equation that describes dynamics near a Hopf bifurcation with delayed feedback [9]

$$\frac{dA}{dt} = (c_1 + ic_2)A - (1 + ic_3)A|A|^2 + \kappa e^{i\phi}(A(t-T) + P(t-T)) \tag{18}$$

for $c_1 > 0$ with the term (10) that accounts for the dispersion in delay line. We study the stability of the CW regime $A(t) = A_0e^{i\nu t}$ in the case of resonant feedback into the maximum gain external cavity mode, where $c_2 = c_3\left(c_1 + e^{-\frac{d\Gamma}{\Gamma^2+\Omega^2}\kappa}\right)$ and $\phi = \frac{d\Omega}{\Gamma^2+\Omega^2}$. Therefore, we obtain

$$A_0^2 = \gamma + \kappa e^{-\frac{\Gamma d}{\Gamma^2+\Omega^2}},$$

and the characteristic equation (13), where

$$a(\lambda) = \kappa^2 e^{-\frac{2\Gamma d}{\Gamma^2+\Omega^2}},$$

$$b(\lambda) = 2\kappa e^{-\frac{(2\Gamma+\lambda)d\left(\Gamma(\Gamma+\lambda)+\Omega^2\right)}{(\Gamma^2+\Omega^2)\left((\Gamma+\lambda)^2+\Omega^2\right)}}\left[\left(2\kappa + e^{\frac{\Gamma d}{\Gamma^2+\Omega^2}}(c_1+\lambda)\right)\cos\Psi + c_3\left(\kappa + e^{\frac{\Gamma d}{\Gamma^2+\Omega^2}}c_1\right)\sin\Psi\right],$$

$$\Psi = \frac{\lambda(2\Gamma+\lambda)d\Omega}{(\Gamma^2+\Omega^2)\left((\Gamma+\lambda)^2+\Omega^2\right)},$$

$$c(\lambda) = 3\kappa^2 e^{-\frac{2\Gamma d}{\Gamma^2+\Omega^2}} + 2\kappa e^{-\frac{\Gamma d}{\Gamma^2+\Omega^2}}(c_1+2\lambda) + \lambda(2\gamma+\lambda).$$

Therefore, for $y(\mu) = -\operatorname{Re}\ln\hat{Y}(\mu)$, $\hat{Y}(\mu) = Y(i\mu)$ we obtain

$$y''(0) = -\frac{1}{\kappa^2 e^{-\frac{2\Gamma d}{\Gamma^2+\Omega^2}}} - D_2 c_3 - \frac{2\Gamma\Omega^3(3\Omega^2-\Gamma^2)}{(\Gamma^2+\Omega^2)^3} + \frac{2\Gamma\Omega^5}{(\Gamma^2+\Omega^2)^4}\left(1+c_3^2\right)\left(1+\frac{\kappa}{c_1 e^{\frac{\Gamma d}{\Gamma^2+\Omega^2}}+\kappa}\right).$$

Finally, we obtain the necessary condition for modulational instability for the mode $\nu = 0$ similarly to the necessary condition for complex Ginzburg-Landau equations and for FDML laser

$$D_2 c_3 < -\frac{1}{\kappa^2 e^{-\frac{2\Gamma d}{\Gamma^2+\Omega^2}}}. \tag{19}$$

# References


[1] D. C. Adler, W. Wieser, F. Trepanier, J. M. Schmitt, and R. A. Huber. Extended coherence length fourier domain mode locked lasers at 1310 nm. *Optics Express*, 19(21):20930–20939, 2011.

[2] S. Boscolo, S. V. Sergeyev, C. Mou, V. Tsatourian, S. Turitsyn, C. Finot, V. Mikhailov, B. Rabin, and P. S. Westbrook. Nonlinear pulse shaping and polarization dynamics in mode-locked fiber lasers. *International Journal of Modern Physics B*, 28(12):1442011, 2014.

[3] D. Brunner, M. C. Soriano, C. R. Mirasso, and I. Fischer. Parallel photonic information processing at gigabyte per second data rates using transient states. *Nature Communications*, 4:1364 EP –, 01 2013.

[4] S. A. Campbell. Time delays in neural systems. In *Handbook of brain connectivity*, pages 65–90. Springer, 2007.

[5] T. Erneux. *Applied delay differential equations*, volume 3. Springer Science & Business Media, 2009.

[6] B. Garbin, J. Javaloyes, G. Tissoni, and S. Barland. Topological solitons as addressable phase bits in a driven laser. *Nature Communications*, 6, 2015.

[7] M. Heuck, S. Blaaberg, and J. Mørk. Theory of passively mode-locked photonic crystal semiconductor lasers. *Optics Express*, 18(17):18003–18014, 2010.

[8] R. Huber, M. Wojtkowski, and J. Fujimoto. Fourier domain mode locking (FDML): A new laser operating regime and applications for optical coherence tomography. *Optics Express*, 14(8):3225–3237, 2006.

[9] L. Jaurigue, E. Schöll, and K. Lüdge. Suppression of noise-induced modulations in multidelay systems. *Phys. Rev. Lett.*, 117:154101, Oct 2016.

[10] H. Kaper and H. Engler. *Mathematics and climate*, volume 131. SIAM, 2013.

[11] B. Kelleher, C. Bonatto, P. Skoda, S. P. Hegarty, and G. Huyet. Excitation regeneration in delay-coupled oscillators. *Phys. Rev. E*, 81:036204, Mar 2010.

[12] G. Kozyreff, A. Vladimirov, and P. Mandel. Global coupling with time delay in an array of semiconductor lasers. *Physical Review Letters*, 85(18):3809, 2000.

[13] R. Lang and K. Kobayashi. External optical feedback effects on semiconductor injection laser properties. *IEEE Journal of Quantum Electronics*, 16(3):347–355, Mar 1980.

[14] D. Levin. Fast integration of rapidly oscillatory functions. *Journal of Computational and Applied Mathematics*, 67(1):95–101, 1996.

[15] M. Marconi, J. Javaloyes, S. Balle, and M. Giudici. How lasing localized structures evolve out of passive mode locking. *Phys. Rev. Lett.*, 112(22):223901, 2014.

[16] M. Marconi, J. Javaloyes, S. Barland, S. Balle, and M. Giudici. Vectorial dissipative solitons in vertical-cavity surface-emitting lasers with delays. *Nature Photonics*, 9(7):450–455, 2015.

[17] T. Nitta. *Complex-Valued Neural Networks: Utilizing High-Dimensional Parameters: Utilizing High-Dimensional Parameters*. IGI Global, 2009.

[18] A. Pimenov, V. Z. Tronciu, U. Bandelow, and A. G. Vladimirov. Dynamical regimes of a multistripe laser array with external off-axis feedback. *JOSA B*, 30(6):1606–1613, 2013.

[19] K. Pyragas. Continuous control of chaos by self-controlling feedback. *Physics Letters A*, 170(6):421 – 428, 1992.

[20] S. Slepneva, B. Kelleher, B. O'Shaughnessy, S. Hegarty, A. G. Vladimirov, and G. Huyet. Dynamics of fourier domain mode-locked lasers. *Opt. Express*, 21(16):19240–19251, 2013.

[21] S. Slepneva, B. O'Shaughnessy, B. Kelleher, S. Hegarty, A. G. Vladimirov, H. Lyu, K. Karnowski, M. Wojtkowski, and G. Huyet. Dynamics of a short cavity swept source oct laser. *Opt. Express*, 22(15):18177–18185, 2014.

[22] H. Smith. *An introduction to delay differential equations with applications to the life sciences*, volume 57. Springer Science & Business Media, 2010.

[23] E. Turitsyna, S. Smirnov, S. Sugavanam, N. Tarasov, X. Shu, S. Babin, E. Podivilov, D. Churkin, G. Falkovich, and S. Turitsyn. The laminar-turbulent transition in a fibre laser. *Nature Photonics*, 7(10):783–786, 2013.

[24] W. van Saarloos and P. Hohenberg. Fronts, pulses, sources and sinks in generalized complex ginzburg-landau equations. *Physica D*, 69:209, 1993.

[25] A. G. Vladimirov, G. Huyet, and A. Pimenov. Delay differential models in multimode laser dynamics: taking chromatic dispersion into account. *Proc. SPIE*, 9892:98920I–98920I–7, 2016.

[26] A. G. Vladimirov and D. Turaev. Model for passive mode-locking in semiconductor lasers. *Phys. Rev. A*, 72:033808 (13 pages), 2005.

[27] S. Yanchuk and M. Wolfrum. A multiple time scale approach to the stability of external cavity modes in the Lang-Kobayashi system using the limit of large delay. *SIAM J. Appl. Dyn. Syst.*, 9:519–535, 2010.

[28] H. C. Yuen and B. M. Lake. Instabilities of Waves on Deep Water. *Annual Review of Fluid Mechanics*, 12:303–334, 1980.

[29] V. E. Zakharov and A. B. Shabat. Exact theory of two-dimensional self-focusing and one-dimensional self-modulation of waves in nonlinear media. *Sov. Phys. JETP*, 34(1):62–69, 1972.